# The Shape and Figure Rotation of NGC 2915's Dark Halo

M. Bureau[1], K. C. Freeman, and D. W. Pfitzner

Mount Stromlo and Siding Spring Observatories, Institute of Advanced Studies, The Australian National University, Private Bag, Weston Creek P.O., ACT 2611, Australia

and

G. R. Meurer

Department of Physics and Astronomy, Johns Hopkins University, Baltimore, MD 21218, U.S.A.

Received _____; accepted _____

Submitted to The Astronomical Journal

[1]Now at Sterrewacht Leiden, Postbus 9513, 2300 RA Leiden, The Netherlands

## ABSTRACT

NGC 2915 is a blue compact dwarf galaxy with a very extended H I disk. This disk shows a short central bar and extended spiral arms, both reaching far beyond the optical component. We use Tremaine & Weinberg's (1984) method to measure the pattern speed of the bar and spiral arms from H I radio synthesis data. Our measurements yield a pattern speed of $\Omega_p = 0.21 \pm 0.06$ km s$^{-1}$ arcsec$^{-1}$ ($8.0 \pm 2.4$ km s$^{-1}$ kpc$^{-1}$ for $D = 5.3$ Mpc), in disagreement with the general view that corotation in barred disks lies just outside the end of the bar, but consistent with recent models of barred galaxies with dense dark matter halos. Our adopted bar semi-length $r_b \approx 180''$ puts corotation at more than 1.7 $r_b$. The existence of the pattern is also problematic. Because NGC 2915 is isolated, gravitational interactions cannot account for the structure observed in the H I disk. We also demonstrate that the low surface density observed in the disk and the location of the pseudo-rings make it unlikely that swing amplification (Toomre 1981) or bar-driven spiral arms could explain the bar and spiral pattern.

Based on the similarity of the dark matter and H I surface density profiles, we discuss the possibility of dark matter distributed in a disk and following closely the H I distribution. This disk then becomes gravitationally unstable and can naturally form a bar and spiral pattern. However, this explanation is difficult to reconcile with some properties of NGC 2915. Finally, we consider the effect of a massive and extended triaxial dark matter halo with a rotating figure. The existence of such halos is supported by CDM simulations showing strongly triaxial dark halos with slow figure rotation. The observed structure of the H I disk can then arise through forcing by the rotating triaxial figure. We associate the measured pattern speed in NGC 2915 with the figure rotation of

its dark halo.

*Subject headings:* cosmology: dark matter — galaxies: evolution — galaxies: formation — galaxies: individual: NGC 2915 — galaxies: kinematics and dynamics — galaxies: structure

## 1. Introduction

About 30% of spiral galaxies are strongly barred. This fraction is roughly doubled if weaker bar-like asymmetries are included, and it reaches almost unity if $K$-band images and quantitative methods are used for classification (see, e.g., Seiger & James 1998). Studying barred spiral galaxies is therefore an important part of galactic structure and dynamics, and we refer the reader to the review by Sellwood & Wilkinson (1993).

The form of the potential and the bar pattern speed ($\Omega_p$) are the most important quantities determining the structure and dynamics of a barred disk. $N$-body simulations of bars (e.g. Sellwood 1981; Combes & Sanders 1981) and analytical calculations (e.g. Contopoulos 1980; Contopoulos & Grosbøl 1989) have shown that for bars to be self-consistent, their pattern speed should be such that corotation occurs outside the end of the bar. However, measuring the pattern speed of bars is not an easy task and most methods are rather indirect (see, e.g., Schwarz 1981, 1984; Athanassoula 1992b; Canzian 1993). The method proposed by Tremaine & Weinberg (1984) is the only direct method, based on observables alone. However, because of the assumptions it makes, the method is rarely applicable to real galaxies and it has been applied successfully to only two objects so far (NGC 936: Kent 1987, Merrifield & Kuijken 1995; NGC 4596: Gerssen, Kuijken, & Merrifield 1999). In this paper, we apply the Tremaine & Weinberg (TW) method to the galaxy NGC 2915, a blue compact dwarf (BCD) galaxy with a very extended H I disk (Meurer, Mackie, & Carignan 1994, hereafter MMC94; Meurer et al. 1996, hereafter MCBF96). This disk shows a late barred spiral galaxy morphology extending far beyond the optical component.

While the formation of bars is now fairly well understood, the formation of the spiral patterns seen in many galaxy disks remains an open issue. Various mechanisms have been proposed to form and maintain spiral patterns. We will consider the most prominent ones

in this paper: gravitational interactions (e.g. Noguchi 1987), swing amplification of spiral density waves (Toomre 1981), and bar-driven spiral arms (e.g. Byrd et al. 1994). We show that none of these is likely to explain the bar and spiral arms structure observed in the H I disk of NGC 2915.

This problem leads us to consider the background mass distribution in NGC 2915. In order to reproduce their flat rotation curves, disks are commonly believed to be immersed in massive dark halos (e.g. Carignan & Freeman 1985). Although the shape of such halos is often assumed to be spherical, there is little observational information on this subject and other shapes are clearly possible (see, e.g., Trimble 1987 and Carr 1994 for reviews). In the case of NGC 2915 in particular, we demonstrate that a simple rigid spherical halo is unable to explain the properties of the H I disk. We therefore consider other dark matter distributions, including: 1) dark matter distributed in a thin disk following the H I surface density distribution, and 2) dark matter distributed in an extended triaxial halo with a slowly rotating figure.

In § 2, we discuss the TW method to measure the pattern speed of bars and review its past applications. In § 3, we describe the properties of NGC 2915 and measure its pattern speed. The issues of self-consistency and multiple pattern speeds are touched upon in § 4, and in § 5 we discuss the possible formation mechanisms for the bar and spiral pattern. We consider two particular models for the dark matter distribution of NGC 2915 in § 6.

## 2. Pattern Speed Measurement

### 2.1. Indirect Methods

Many indirect methods have been devised to measure the bar pattern speed $\Omega_p$ in barred spiral galaxies, and we discuss two of them here. The first one relies on the theory

of resonance ring formation (Schwarz 1981, 1984; see also Byrd, Ousley, & Dalla Piazza 1998). It is possible to identify morphological features in the disk of a barred galaxy, such as rings, with the locations of known resonances. Using the circular velocity curve and derived epicyclic frequency, the bar pattern speed can then be inferred (see, e.g., Ryder et al. 1996 for recent applications to NGC 1433 and NGC 6300). We apply this method to NGC 2915 in § 5. Second, it is possible to construct hydrodynamical models of the gas flow in a galaxy (often to reproduce H I observations because of their full kinematical coverage). Hydrodynamical models depend on several parameters of the potential, including $\Omega_p$, so the best fitting model gives an estimate of the bar pattern (see, e.g., Lindblad & Kristen 1996 and Lindblad, Lindblad, & Athanassoula 1996 for recent applications to NGC 1300 and NGC 1365). Sellwood & Wilkinson (1993) review many such barred galaxy studies.

Although these indirect methods yield useful information about pattern speeds, it is clearly preferable to have a direct measurement, with no dependence on theoretical arguments or comparison with dynamical models. We will thus pursue these indirect methods only as a consistency check of more direct measurements.

### 2.2. Direct Methods

Tremaine & Weinberg (1984) showed that the pattern speed of a barred disk galaxy can be derived from the observed kinematics of a tracer population if (1) there exists a unique, well-defined disk pattern speed $\Omega_p$, and (2) the luminosity density of the tracer satisfies the continuity equation. With these conditions, the pattern speed is given by

$$\Omega_p \sin i = \frac{\int_{-\infty}^{\infty} h(y)dy \int_{-\infty}^{\infty} \Sigma(x,y)[\bar{v}_{los}(x,y) - v_{sys}]dx}{\int_{-\infty}^{\infty} h(y)dy \int_{-\infty}^{\infty} \Sigma(x,y)xdx}, \quad (1)$$

where $i$ is the disk inclination, $\Sigma$ is the surface brightness distribution of the tracer, $\bar{v}_{los}$ is the mean line-of-sight velocity of the tracer, $v_{sys}$ is the systemic velocity of the galaxy,

and $(x, y)$ are Cartesian coordinates on the plane of the sky, with the origin at the center of the galaxy and the $x$-axis parallel to the line of nodes (i.e. the apparent major axis for an intrinsically round disk). These quantities are all observables. The function $h(y)$ is an arbitrary weighting function (see Tremaine & Weinberg 1984). Although the method was intended to measure bar pattern speeds, it can equally be applied to any strong and fairly open pattern, such as spiral arms.

The continuity assumption is valid for dust-free old stellar populations, but may well break down in dusty systems, or when using gas as a tracer (possibility of ionisation, molecular conversion, optical thickness, etc.). In fact, while Tremaine & Weinberg (1984) succeeded in applying their method to an artificial dataset generated from an $N$-body simulation, they failed on H I data from the barred spiral galaxy NGC 5383 (Sancisi, Allen, & Sullivan 1979). The method is fairly sensitive to noise because only the non-symmetric (i.e. odd in $x$) part of $\Sigma$ contributes to the integrals in equation (1).

Kent (1987) applied the TW method to the barred spiral galaxy NGC 936. The stellar component of NGC 936 is ideal for this application because it has a strong bar, high surface brightness, high rotation velocity, and is devoid of dust and star formation. The orientation of the system is also favourable. Kent carefully estimated the sources of error in measuring $\Omega_p$. Unfortunately, the relatively poor quality of the kinematical data (by today's standards) led to inconclusive results. He derived an average pattern speed of $\Omega_p = 8.4 \pm 2.9$ km s$^{-1}$ arcsec$^{-1}$ ($\Omega_p = 104 \pm 36$ km s$^{-1}$ kpc$^{-1}$ for $D = 16.6$ Mpc). With Kormendy's (1984) rotation curve, corrected for non-circular motions, and a deprojected bar length of $52''$, corotation then lies between 0.54 and 1.21 bar semi-lengths. This is only marginally consistent with the general result from orbital calculations and self-consistent models of barred spiral galaxies, that corotation must occur outside the end of the bar and is generally located just beyond its ends (see e.g. Sellwood 1981; Teuben & Sanders 1985;

Athanassoula 1992b).

Merrifield & Kuijken (1995; see also Kuijken & Merrifield 1996) reapplied the TW method to NGC 936, this time with better data and methods. They did not use equation (1) directly, but rather used the equivalent formula

$$\Omega_p \sin i = \frac{\langle \bar{v}_{los} \rangle - v_{sys}}{\langle x \rangle} \quad \text{(for a given } y\text{)}, \tag{2}$$

where the brackets represent luminosity-weighted averages along the slit. The advantage of this procedure is that the long-slit data can be co-added along the spatial axis to measure $\langle \bar{v}_{los} \rangle$, and along the dispersion axis to measure $\langle x \rangle$, yielding higher signal-to-noise measurements. To obtain an unbiased measure of $\langle \bar{v}_{los} \rangle$, Merrifield & Kuijken (1995) also used a deconvolution algorithm allowing for asymmetric Doppler broadening of the spectral lines. They obtained a well-defined average pattern speed of $\Omega_p = 4.8 \pm 1.1$ km s$^{-1}$ arcsec$^{-1}$ ($\Omega_p = 60 \pm 14$ km s$^{-1}$ kpc$^{-1}$ for $D = 16.6$ Mpc). This value puts corotation at $69 \pm 15''$, or $1.3 \pm 0.3$ bar radii, in good agreement with theoretical expectations.

Using the same procedure, Gerssen, Kuijken, & Merrifield (1999) recently measured the bar pattern speed in the SBa galaxy NGC 4596, which is similar to NGC 936. They derive a pattern speed of $\Omega_p = 3.9 \pm 1.0$ km s$^{-1}$ arcsec$^{-1}$ ($\Omega_p = 52 \pm 13$ km s$^{-1}$ kpc$^{-1}$ for $D = 15.7$ Mpc). This again indicates a fast bar, placing corotation just outside the end of the bar, at approximately 1.25 bar semi-lengths (see also Kent 1990).

## 3. NGC 2915

### 3.1. Background

EDITOR: PLACE TABLE 1 HERE.

NGC 2915 is a nearby relatively isolated BCD galaxy. MMC94 carried out optical

imaging and spectroscopy of NGC 2915 to study its structure, stellar populations, and star formation history. MCBF96 obtained H I synthesis data to study the neutral hydrogen distribution and kinematics, and NGC 2915's overall mass distribution (including dark matter). Table 1 summarises the basic properties of NGC 2915.

The photometry of MMC94 shows that NGC 2915 has two distinct stellar populations: (1) an exponential red diffuse population in the outer parts ($r \geq 35'' = 0.90$ kpc), with a scale length $\alpha_B^{-1} = 25\farcs6$ (660 pc), an extrapolated central surface brightness $B(0)_c = 22.44$ mag arcsec$^{-2}$ (corrected for inclination and extinction), and constant color; and (2) a slightly peaked core population ($r < 35''$), with increasingly bluer color toward the center. The diffuse population is similar to that of dwarf elliptical galaxies, but the core is lumpy, contains a young stellar population, and is the locus of high mass star formation. Spectroscopy in the core shows strong Balmer and Ca II H+K absorption lines, and strong narrow emission lines with ratios typical of high excitation low metallicity H II regions. A velocity difference of 60 km s$^{-1}$ is detected across the inner galaxy. If this gradient is due solely to rotation, it corresponds to a deprojected rotational velocity of $V_r = 50 \pm 21$ km s$^{-1}$ at $r = 32''$ (neglecting the effects of the bubbles seen in H$\alpha$ by Marlowe et al. (1995)). The associated mass $M_{\rm Core} = 4.8 \times 10^8\ M_\odot$ for the optical core, with a mass-to-light ratio $M_{\rm Core}/L_B = 1.3\ M_\odot/L_{B,\odot}$.

EDITOR: PLACE TABLE 2 HERE.

EDITOR: PLACE FIGURE 1 HERE.

EDITOR: PLACE FIGURE 2 HERE.

The neutral hydrogen observations of NGC 2915 (MCBF96) reveal an H I distribution very different from the optical. Figure 1 shows the naturally weighted total H I intensity map overlaid on an optical image of NGC 2915. The H I distribution is unusually extended, up to 5 $D_{\rm Ho,B}$ (22.6 $\alpha_B^{-1}$), and it has a striking late-type barred spiral galaxy morphology, with two extended spiral arms starting at the end of a central bar. This is unusual as bars are generally H I poor. At higher resolution, the H I bar is resolved into two clouds; its semi-length is about 2.′4 (3.7 kpc), and it corresponds roughly in position, orientation, and size to the optical emission. The H I surface density profile is tabulated in Table 2. The total H I mass is $M_{\rm HI} = 9.6 \times 10^8\ M_\odot$, while the H I mass in the bar is only about $5 - 7.5 \times 10^7\ M_\odot$. Figure 2 shows the MCBF96 naturally weighted H I velocity field of NGC 2915, again overlaid on an optical image. It clearly shows the pattern of a rotating disk (with an oval distortion), and suggests the presence of a warp in the outer parts. MCBF96 derived a rotation curve for NGC 2915 using the standard tilted ring algorithm ROTCUR (Begeman 1989). The position angle varies by about 15° and the inclination by about 10° outside of the barred region (where the effects of the bar and a possible warp are hard to disentangle), supporting the presence of a warp in the outer disk. The H I velocity dispersion outside the bar region is the usual $\sigma_v \approx 8$ km s$^{-1}$, but it increases up to 40 km s$^{-1}$ in the central regions (see Table 2), a value comparable to the rotation velocities obtained from ROTCUR. This indicates that pressure support is important in the center. MCBF96 applied an asymmetric drift correction to the rotation curve to produce the "circular velocity curve" needed for mass modelling. The circular velocity is tabulated in Table 2. It increases rapidly with radius in the inner parts, reaching 80 km s$^{-1}$ by $r = 150''$ (3.9 kpc), stays flat until $r = 400 - 450''$ (10.3-11.6 kpc), and increases again up to ≈90 km s$^{-1}$ at the last measured point ($r \approx 600'' = 15.4$ kpc).

MCBF96 constructed three-component mass models to interpret the circular velocity curve. The models were composed of: (1) a stellar disk, obtained from the surface

brightness profiles of MMC94 (the mass-to-light ratio $M/L_B$ is a free parameter); (2) an H I disk, based on their observations; and (3) a spherical dark halo (two density distributions were used, both with a central density $\rho_0$ and core radius $r_c$ as free parameters). All models are dominated by dark matter at all radii. In fact, NGC 2915 is one of the "darkest" disk galaxies known. Its dark matter core is very dense and compact, which may prove crucial to understand its pattern speed (see § 4.1). MCBF96's best fit model[2] has $M/L_B = 1.2\ M_\odot/L_{B,\odot}$, $\rho_0 = 0.10 \pm 0.02\ M_\odot\ \mathrm{pc}^{-3}$, and $r_c = 1.23 \pm 0.15$ kpc, yielding a total mass $M_T = 2.7 \times 10^{10}\ M_\odot$, $M_T/L_B = 76\ M_\odot/L_{B,\odot}$, and $M_{dark}/M_{luminous} = 19$ within the last measured point.

### 3.2. Pattern Speed

We now attempt to measure the pattern speed $\Omega_p$ of the figure in the disk of NGC 2915 using the H I data of MCBF96. As mentioned in § 2.2, the continuity equation imposes a strong constraint on the applicability of the TW method, and gaseous systems are usually thought to be poor candidates for a measurement. NGC 2915 is an unusual galaxy, however, and we argue that the TW method should work for its H I distribution. Firstly, because the stellar component of NGC 2915 is confined to the inner regions of its H I distribution, and the star-forming core to the very center of the H I bar, there is no source of ionising photons over most of the H I disk (except for the weak metagalactic radiation field, and possibly some radiation from the distant core reaching the warped regions). Meurer et al. (1999) searched for H II regions in the outer disk, but found none. This situation is in contrast to that in NGC 5383, where Tremaine & Weinberg (1984) failed to obtain a reliable measurement of the pattern speed using neutral hydrogen observations. Furthermore,

[2]Their model D, with a dark matter density distribution $\rho(r) = \rho_0[1 + (r/r_c)^2]^{-1}$.

the H I column density is low enough in most of the disk (where the velocity dispersion $\sigma_v \approx 8$ km s$^{-1}$) that optical thickness problems should not affect the observed H I intensity. Only in the inner parts of the bar, where the optical disk lies, does the column density reach $N_{HI} = 10^{21}$ cm$^{-2}$, but there the H I velocity dispersion is larger ($\sigma_v \approx$ 20-40 km s$^{-1}$), so again the optical thickness is expected to be low. No molecular data on NGC 2915 are available in the litterature, so we do not have any information on possible H I-molecule conversion at this point. However, the low H I column density again suggests that this effect is not important. In order to properly constrain its molecular content, we are nevertheless pursuing molecular line observations of NGC 2915. For all these reasons, and because the bar and spiral arm pattern is clear and strong, we believe that the TW method applied to the H I synthesis data of NGC 2915 should give a realistic measure of its pattern speed. We note that the orientation of the system is ideal, with the disk at intermediate inclination and the bar about 30° from the major axis of the disk.

EDITOR: PLACE FIGURE 3 HERE.

EDITOR: PLACE FIGURE 4 HERE.

We apply the TW method to NGC 2915 using MCBF96's naturally weighted total H I intensity map and velocity field (see Fig. 1 and 2). Additional structural and kinematical parameters are required to use the TW method (see § 2.2), but these are all provided by the tilted-ring analysis of MCBF96. We use averages of their parameters for the outer disk, outside of the barred region ($r > 150''$): the center of the disk $(x_c, y_c) = (0'', 0'')$ (with respect to the pointing center of $\alpha = 9^{\rm h}26^{\rm m}11^{\rm s}$, $\delta = -76\,{\rm deg}\,37'35''$), $v_{sys} = 467$ km s$^{-1}$, and the position angle of the line of nodes PA = 117°. We use equation (1) directly, without a weighting function $h(y)$, and for all possible positions $y$ (equivalent to using

$h(y) = \delta(y - y_o)$ for each $y_o$). Because the major axis traces the position of the line of nodes, $y$ is effectively the position of the integration axis along the minor axis of the galaxy. Each offset $y$ provides an independent measurement of the pattern speed. The coordinate system is shown in Figure 3, and Figure 4a shows the derived pattern speed as a function of the offset $y$. The measurements are roughly consistent with each other for most offsets. Only for a few isolated points and for offsets between 0 and 200″ on the NW side of the galaxy (positive offsets) are the values of $\Omega_p \sin i$ significantly discrepant (but see below). We recall that the TW method assumes a unique pattern speed for the whole disk, so all offsets should yield similar pattern speeds.

The discrepant region is associated with the northernmost of the two clouds identified by MCBF96, located at the northern end of the bar. Around that region, both the total H I intensity distribution and the velocity field show a strong deviation from their largescale pattern. The discrepancies in the derived pattern speeds probably arise from the fact that the cloud breaks the pattern in the density distribution and/or the velocity field, an effect to which equation (1) is very sensitive. Away from this problematic region, the pattern speed is well-defined: the entire SE half of the galaxy and the farthest regions in the NW half both yield fairly consistent values for $\Omega_p \sin i$. We thus believe that the TW method works using the H I component of NGC 2915 and gives a reliable estimate its the pattern speed.

In our calculations, we assumed that the parameters required to use the TW method were fixed over the whole disk. The center of the disk is well-defined, and only the x-component of the center ($x_c$) affects the calculations anyway. The systemic velocity is also well constrained, with a small uncertainty of a few km $s^{-1}$. However, as shown by the tilted-ring analysis of MCBF96, both the inclination $i$ and position angle PA vary significantly with radius in NGC 2915. A change in inclination only affects the pattern speed

measurements through the deprojection, but a change in position angle materially affects the calculations themselves. We have therefore reapplied the TW method to the H I data using a range of values for $x_c$, $v_{sys}$, and PA. Although no combination of parameters yields perfectly equal pattern speeds for all offsets, most cases with plausible values show a regular behaviour, with only a restricted range of offsets having very discrepant measurements.

A typical good case is presented in Figure 4b. For all combinations of parameters, the flat portions of the $\Omega_p \sin i$ "distribution" always lie between $\Omega_p \sin i = 0.12$ km s$^{-1}$ arcsec$^{-1}$ and $\Omega_p \sin i = 0.22$ km s$^{-1}$ arcsec$^{-1}$. We therefore adopt $\Omega_p \sin i = 0.17 \pm 0.05$ km s$^{-1}$ arcsec$^{-1}$ ($\Omega_p \sin i = 6.6 \pm 1.9$ km s$^{-1}$ kpc$^{-1}$ for $D = 5.3$ Mpc) as our estimate of the pattern speed in NGC 2915. The uncertainty given represents half the range of measured values for $\Omega_p \sin i$, and is not a standard error estimate. It is clear from our measurements that formal errors are much smaller than the errors introduced by the uncertainties in the structural and kinematical parameters of the disk, or the errors introduced by the fact that we are working with a less-than-perfect system. From the outer parts of the disk again, we get an average inclination $i = 56 \pm 3°$. This gives a deprojected pattern speed $\Omega_p = 0.21 \pm 0.06$ km s$^{-1}$ arcsec$^{-1}$ ($8.0 \pm 2.4$ km s$^{-1}$ kpc$^{-1}$).

The 30% uncertainty in $\Omega_p$ is comparable to that achieved by Merrifield & Kuijken (1995) for NGC 936, but is still large given that we are using gas kinematics with the advantage of complete two-dimensional spatial coverage. On the other hand, our error estimate (half the range of measured values) is very conservative. As suggested by Tremaine & Weinberg (1984), we tried using odd weighting functions (e.g. $h(y) = \delta(y - y_0) - \delta(y + y_0)$; $y_c$ now affecting the calculations directly). Such weighting eliminates the contribution of perturbations with odd azimuthal wavenumbers to the integrals in equation (1), and diminishes the effect of centering errors. However, it did not improve our results, because discrepant regions on one side of the minor axis contaminate the combined measurements

from both sides. Although we cannot exclude the possibility that the continuity equation is not fully satisfied for the H I in some parts of NGC 2915 (particularly the central regions), the main sources of uncertainty in our measurements are the poorly constrained disk parameters (mainly PA), in turn related to the presence of a strong warp in the outer disk. Tremaine & Weinberg (1984) note that a warp may affect the pattern speed determination, acting as a non-axisymmetric perturbation with zero pattern speed. There may be some short-lived features in the disk (such as the structure seen near the NW cloud), but their effect is hard to quantify. We repeated the calculations using only the inner barred region of the galaxy, but the results were inconclusive. It is far from clear that the method should work in such a case anyway, as the integrals in eq. [1] should extend over the whole system.

## 4. The Nature of the Pattern

### 4.1. Self-Consistent Bars

Orbital calculations in barred disk potentials show that bars should end at or inside their corotation radius (see, e.g., Contopoulos 1980; Athanassoula 1992a; for a review see Contopoulos & Grosbøl 1989). The argument is that the bar-shaped $x_1$ orbits, believed to support self-consistent bars, extend close to but not past corotation.

$N$-body studies show that rotationally supported stellar disks are globally unstable to bi-symmetric distortions and quickly form strong bars. This is seen in both two-dimensional (e.g. Sellwood 1981; Athanassoula & Sellwood 1986) and three-dimensional (e.g. Combes & Sanders 1981; Raha et al. 1991) simulations. These instabilities can be identified with the dominant linear modes found in analytical global stability analyses of axisymmetric disks (e.g. Kalnajs 1971, 1977). The main characteristic of the stellar bars formed in such simulations is that the they are fast, generally ending at or just inside corotation (where

$\Omega_p = \Omega(r)$).

This property of self-consistent barred disks does not appear to hold in NGC 2915; the gaseous bar ends well within corotation. We take the ends of the bar to be where the density of the rectangular-shaped central component of the H I distribution drops rapidly. This is also the region where the spiral arms start. The observed semi-length of the bar is then about 145″, with a deprojected value of $r_b \approx 180''$. Our adopted pattern speed $\Omega_p = 0.21 \pm 0.06$ km s$^{-1}$ arcsec$^{-1}$ (see § 3.2) and MCBF96's circular velocity curve (see Table 2) put corotation at a radius $r_{co} = 390^{+\infty}_{-80}$ arcsec (see Fig. 7). The ratio of corotation to the bar semi-length is thus very large, $r_{co}/r_b > 1.7$, indicating a *slowly* rotating bar.

Such a slow pattern speed is inconsistent with the the simulations mentioned above. However, all these studies used models where luminous mass dominates the inner (optical) regions of the galaxies. MCBF96 showed that this is not the case in NGC 2915, where dark matter dominates at all radii. In fact, the dense and compact dark matter core of NGC 2915 may be the clue to its slow pattern speed. Dense dark halos have been predicted to slow down bars significantly, as the bar can transfer angular momentum to the outer disk and halo efficiently through dynamical friction (see Sellwood 1980; Weinberg 1985; Debattista & Sellwood 1998). Because dak matter is generally more important in late-type spirals, where it is difficult to measure pattern speeds, present support for these models is marginal (see, e.g., Elmegreen 1996). NGC 2915 may thus represent the strongest observational evidence so far for bar deceleration by dark halos with high central densities. The mass model of MCBF96, the $N$-body simulations of Debattista & Sellwood (1998), and the bar pattern speed measured here are all consistent with each other. However, the effects of gaseous processes on bar deceleration remain to be fully investigated. These have not been taken into account in the aforementioned studies, but are certainly relevant in the case of NGC 2915. Gas inflow, in particular, could lead to a speed up of the bar.

### 4.2. Bar or Spiral Arms Pattern Speed?

The TW method measures the pattern speed of a disk, assumed to be unique. While it was designed to measure bar pattern speeds, it equally applies to any pattern present in the disk, as long as it is strong enough. It is therefore important to establish which component's pattern speed we are measuring. Are we measuring the pattern speed of the bar, the spiral arms, or a common pattern speed for both?

Sellwood & Sparke (1988) suggest that spiral arms in barred spiral galaxies could have a different (lower) pattern speed than the bar. Their work was aimed primarily at explaining the presence of dust lanes on the inner edge of spiral arms in many objects. A lower pattern speed for the spiral pattern would allow the gas to overtake that pattern and therefore lie within its corotation radius in that region, while still retaining the view that bars end just inside *their* corotation radius. Sellwood & Sparke (1988) suggestion is supported by $N$-body simulations of barred galaxies showing outer spiral patterns slower than the bars (e.g. Sparke & Sellwood 1987).

Tagger et al. (1987) and Sygnet et al. (1988) develop the idea that the non-linear coupling of modes with different pattern speeds could sustain spiral structures for a long time. For the mechanism to be efficient, resonances of the two patterns must be closely spaced. They observe this effect in many $N$-body simulations, where the corotation radius of the bar and the inner Lindblad resonance (ILR) of the spiral pattern are very close (this is also the region where the bar ends and the spiral arms begin). The beat wave generated is then axisymmetric and close to its Lindblad resonance and it couples non-linearly to the bar and spiral arms.

If we assume that the pattern speed measured here is that of the spiral arms, and that the corotation radius of the bar lies close to the ILR of the spiral pattern, as suggested by Tagger et al. (1987) and Sygnet et al. (1988), we obtain a bar corotation radius $r_{co} < 50''$

(see Fig. 7), well inside the bar observed in H I ($r_b \approx 180''$). Such a view would be difficult to defend, considering the body of analytical and numerical work which requires the corotation radius to lie at or beyond the end of the bar. This is a strong indication that we are in fact measuring the pattern speed of the bar.

Furthermore, considering the form of equation (1), we see that for small minor axis offsets ($y < 90''$) both the central (barred) and external (non-barred) regions of the galaxy contribute to the integrals, while for large offsets ($y > 90''$), the integration axis does not cross the barred region and only the outer parts of the disk contribute to the pattern speed calculations. If the bar and spiral arms had significantly different pattern speeds, we would expect the TW method to fail for small offsets. However, excluding the discrepant points 0-200″ on the NW side of the galaxy (which we attribute to a large H I cloud, see § 3.2), the pattern speed measurements yield a relatively constant value for all offsets and for most reasonable combinations of parameters. Considering the relatively small extent of the barred region and the importance of the flux in the outer parts of the disk, it might appear that the spiral arms dominate the contribution to the integrals in equation (1) even in the central regions. This is not so, however. For small offsets, both the inner barred region and the outer parts of the disk contribute significantly to the numerator. It is therefore very likely that a unique pattern speed is being measured. This view is further strengthened by the fact that the spiral arms in NGC 2915 appear to start from the end of the bar (although Sellwood & Sparke (1988) showed that this is not a strong argument).

We therefore adopt the view that the pattern speed which we have measured in § 3.2 *is* the unique, common pattern speed of both the bar and the spiral arms, although we cannot entirely exclude the possibility that it is the pattern speed of the spiral arms alone.

## 5. The Origin of the Pattern

Many theories exist to explain the formation of bar and spiral patterns in disk galaxies. We will now focus on some of these. We note that the issue of the origin of the pattern in NGC 2915 is largely indepedent of the measured pattern speed. For example, is the pattern a phenomenon of the disk itself, or is it driven by other effects? We will show that the existence of a pattern in NGC 2915 is somewhat problematic.

### 5.1. Gravitational Interactions

Tidal triggering is a potentially important way to form bars, especially in dense environments. In the case of parabolic prograde planar encounters, Noguchi (1987) finds that self-consistent disks (with a static halo) develop strong spiral structures over their entire length, with a bar-like pattern in the inner regions. Gerin, Combes, & Athanassoula (1990) show that interaction with a companion accelerates bar formation. The sense of interaction (prograde or retrograde) affects the bar growth rate and shape, with lesser effects on the strength and pattern speed of the resulting bar. When a bar already exists, its strength and pattern speed can again be affected by an interaction.

It seems unlikely that such interaction scenarios can explain the structure seen in the H I disk of NGC 2915. No evidence of interaction is seen in the H I data of MCBF96, and the only catalogued potential interaction partner for NGC 2915 within 5° is a low luminosity, low surface brightness object, SGC 0938.1-7623, at a radius of 42′ (projected distance of 65 kpc at the distance of NGC 2915). This object does not have a catalogued optical or H I velocity however, so although there are no indications that NGC 2915 is interacting, we cannot definitively exclude this possibility.

### 5.2. Swing Amplification

EDITOR: PLACE FIGURE 5 HERE.

Swing amplification (Toomre 1981) can generate spiral arms in a disk as transient tidal features. Although Toomre (1981) considered a stellar disk, his treatment should equally apply to gaseous disks. Swing amplification is a local cooperative effect: shear, epicyclic motions, and self-gravity all contribute to support the spiral pattern, originally excited by a small disturbance. In short, the epicyclic motions resonate with the shear flow as the spiral pattern wraps, and the spiral arms are sustained. The self-gravity of the arms then leads to a gravitational instability (Goldreich & Lynden-Bell 1965). The effect can be summarised (somewhat simplified by neglecting the shear) in Toomre's parameter $X$, given by

$$X = \frac{\lambda}{\lambda_{\rm crit}}, \tag{3}$$

where

$$\lambda_{\rm crit} = \frac{4\pi^2 {\rm G}\mu}{\kappa^2}, \tag{4}$$

$\mu$ is the surface density, and $\kappa$ is the epicyclic frequency. Swing amplification is efficient for $X \lesssim 3$ (taking into account the effect of shear and random motions; see, e.g., Fig. 7 of Toomre 1981). For an extended disk, we can write $\lambda = 2\pi r/m$, where $m$ is the azimuthal wavenumber of the spiral pattern considered, and

$$X(r) = \frac{r\kappa(r)^2}{2\pi {\rm G} m \mu(r)} \tag{5}$$

(see Athanassoula, Bosma, & Papaioannou 1987).

Figure 5 shows $X(r)$ for NGC 2915 for two and four-armed spiral patterns. We use here the surface density of the luminous matter only (gaseous and stellar), assuming that the dark matter is not responsive to the density perturbation created by the spiral

pattern (Toomre 1981 considered a fixed halo). In Figure 5a, only the H I distribution from MCBF96 is included (uncorrected for inclination; see Table 2). It is clear from the figure that $X(r)$ is nowhere near a value of 3. In fact, even for $m = 4$, $X(r) \gtrsim 10$ for almost all radii. In Figure 5b, the stellar content is also included. To construct the surface density profile, we used the $B$ surface brightness profile of MMC94 for $r < 125''$, and an extrapolation of their exponential fit to the outer parts of the disk for larger radii: $B_c = 21.79$ mag arcsec$^{-2}$ (corrected for extinction but not inclination) and $\alpha_B^{-1} = 25''.6$, with $M/L_B = 1.2\ M_\odot/L_{B,\odot}$ (as in the adopted mass model of MCBF96). The resulting surface brightness profile is tabulated in Table 2. Even with the stellar component, $X(r) \gtrsim 10$ for most radii (any correction for inclination would further decrease the importance of luminous matter). Small values of $X(r)$ are present in the inner regions only: $X(r) \leq 5$ for $r < 75''$ only. We note however that those regions are within the rapidly rising portion of the rotation curve, where the bar resides and the shear is low, while swing amplification relies on shear to amplify the spiral pattern.

The work by Toomre (1981) refers to a flat rotation curve, $V_c(r) =$ constant, which is not exactly the case here. The amplification criterion $X \lesssim 3$ increases for higher shear rates (e.g. $X \lesssim 6$ for a Keplerian rotation curve, $V_c(r) \propto r^{-1/2}$) and decreases for smaller shear (e.g. $X \lesssim 1.5$ for $V_c(r) \propto r^{1/2}$; Toomre, private communication). So, if anything, the constraints on swing amplification are even stronger in the case of NGC 2915, especially in the inner parts.

EDITOR: PLACE FIGURE 6 HERE.

Toomre's (1964) stability parameter $Q$ also affects the efficiency of the swing amplifier mechanism. The stellar disk of NGC 2915 does not extend into the spiral pattern region, so

we consider only the gaseous disk. Then,

$$Q(r) = \frac{v_s(r)\kappa(r)}{\pi \mathrm{G}\mu(r)}, \tag{6}$$

where $v_s$ is the sound speed of the gas, taken here as the velocity dispersion. As $Q$ increases, the maximum swing amplification factor decreases. For $V_c(r) =$ constant, $Q \gtrsim 2$ curbs most of the amplification (see, again, Fig. 7 of Toomre 1981). The criterion becomes $Q \gtrsim 3$ for $V_c(r) \propto r^{-1/2}$ and $Q \gtrsim 1.5$ for $V_c(r) \propto r^{1/2}$ (Toomre, private communication). Figure 6 shows $Q(r)$ for NGC 2915 using both a constant velocity dispersion, equal to the velocity dispersion in the outer parts of the H I disk, and the H I velocity dispersion profile of MCBF96, tabulated in Table 2. We see that $Q(r) \gtrsim 5$ everywhere, so the amplification factor would be small. In particular, $Q$ is high in the inner regions. The sound speed would have to be less than 2-3 km s$^{-1}$ to make $Q < 2$ over a significant range of radii. Even then, $X$ would still be too high for the swing amplifier to work efficiently.

Given the behaviour of $X(r)$ and $Q(r)$, and if the analogy between Toomre's (1981) stellar treatment and the gaseous treatment adopted here is at least qualitatively valid[3], it is clear that swing amplification cannot explain the spiral pattern seen in the disk of NGC 2915. We note that both $X$ and $Q$ scale inversely with the distance adopted, so a large error in the distance could weaken or invalidate our conclusion (if the real distance is larger). However, the error estimate of MMC94 does not allow this (they quote $D = 5.3 \pm 1.6$ Mpc). A distance of at least 10–15 Mpc would be required to make swing amplification efficient. Furthermore, given the very extended mass distribution of NGC 2915, it is unlikely that the observed spiral pattern results from an edge-mode, as discussed by Toomre (1981).

---

[3]As mentioned by Toomre (1981) based on the work of Bardeen (1975) and Aoki, Noguchi, & Iye (1979), gaseous disks are probably more stable than stellar ones, which would strengthen our conclusions.

At this point, we conclude that the bar and spiral patterns in NGC 2915 are unlikely to be caused by gravitational interaction or swing amplification. We must therefore search for an alternative formation mechanism.

### 5.3. Resonance Ring Formation

EDITOR: PLACE FIGURE 7 HERE.

The arms of spiral galaxies frequently wrap to form ring-like structures. The theory of resonance ring formation (Schwarz 1981, 1984; Byrd et al. 1994) relates the shapes and positions of the rings to the presence of resonances in the disks. An examination of the total H I map of NGC 2915 suggests the presence of two such rings. For a given rotation curve, the bar pattern speed determines the existence and position of the resonances, and therefore the kind and extent of the orbit families present in the disk (Sellwood & Wilkinson 1993). We can thus use resonance ring theory to see if our pattern speed measurement is consistent with the location of the (pseudo-)rings seen in NGC 2915, and determine whether the spiral arms are driven by the bar.

Using MCBF96 circular velocity curve, we can calculate the angular frequency of circular motion $\Omega$ and the associated Lindblad precession frequencies $\Omega + \kappa/2$, $\Omega - \kappa/2$, and $\Omega - \kappa/4$ (see Table 2). These are shown in Figure 7, along with the measured pattern speed and the position of the pseudo-rings in the disk of NGC 2915.

The innermost points in Figure 7 are affected by beam smoothing but suggest the presence of an ILR ($\Omega_p = \Omega - \kappa/2$) at $r < 50''$. Nuclear rings are believed to be associated with ILRs, and usually form easily recognisable annuli of H II regions in the inner parts of galaxies. The shallower the rotation curve in the inner parts, the larger the nuclear ring formed (Byrd et al. 1994). However, no such ring is visible in the photometry of MMC94

or in the Fabry-Perot H$\alpha$ images of Marlowe et al. (1995). The resolution of MCBF96 H I data is too low to resolve a ring of radius smaller than about 1.′5.

The inner spiral arms seen in the total H I intensity map of NGC 2915 (Fig. 3) appear to form a pseudo-ring just outside the end of the bar, at a deprojected radius of $215 \pm 15''$. Inner rings are usually associated with the inner second-harmonic resonance ($\Omega_p = \Omega - \kappa/4$) which, in this case, occurs between about $190''$ and $340''$. This is just consistent with the position of the inner pseudo-ring.

The outer spiral arms seen at the edge of the H I disk in Figure 3 form an outer pseudo-ring at $r = 400 \pm 15''$. Outer rings are associated with the outer Lindblad resonance ($\Omega_p = \Omega + \kappa/2$). However, the $\Omega + \kappa/2$ curve in Figure 7 does not intersect the range of measured values for $\Omega_p$, which suggests that no outer Lindblad resonance is present in the disk of NGC 2915. Therefore, no outer ring would be expected.

Resonance ring theory has only limited success in explaining the position of the various (pseudo-)rings in NGC 2915 (nuclear, inner, and outer rings). It could be that the pattern in NGC 2915 is still evolving, and that the spiral arms are still in the process of forming rings. This seems unlikely, however, since no nuclear ring is detected, and the timescale for the formation of nuclear rings is very short ($10^7$ – $10^8$ yr; Combes 1993). Stellar mass loss or gas infall can also delay the formation of rings (Schwarz 1981), but these are improbable as most of the H I disk is devoid of stars and NGC 2915 is isolated.

Petrou & Papayannopoulos (1986) proposed a mechanism to terminate bars well within their corotation radius. This mechanism requires the presence of a 1:1 resonance ($\Omega_p = \Omega - \kappa$) in the bar, however, so it is clear from Figure 7 that it is not relevant in the case of NGC 2915.

We conclude that the structures seen in the disk of NGC 2915 are probably not due to

resonances and that the spiral pattern is not driven by the bar. In fact, from the positions of the inner and outer pseudo-rings, no single value of the pattern speed can be derived from resonance ring theory.

## 6. Dark Matter and the Structure of NGC 2915

The mass model of MCBF96 showed that NGC 2915 is dominated by dark matter, even in the central (optical) regions of its disk. We now discuss the possible relations between the properties of this dominant dark matter distribution and the properties of the H I pattern.

### 6.1. Rotationally Supported Disk Dark Matter

Pfenniger, Combes, & Martinet (1994; see also Pfenniger & Combes 1994) propose that the dark matter required dynamically in disk galaxies is in the form of rotationally supported cold molecular gas. This idea is attractive for NGC 2915 as it would also provide the extra disk mass needed to explain the formation of the bar and spiral arms through gravitational instabilities. Unfortunately, observing such cold gas directly is difficult (for $H_2$, see Combes & Pfenniger 1997; for CO, see Lequeux & Allen 1993 and Wilson & Mauersberger 1994).

EDITOR: PLACE FIGURE 8 HERE.

Figure 8a shows how much additional mass is required in the *disk* for the swing amplification mechanism to be efficient ($X = 3$ everywhere in the disk; see § 5.2). Similarly, Figure 8b shows how much additional disk matter is required to lower $Q$ to a value of 2 at all radii (the value required to make the disk gravitationally responsive). Again, those two

values scale inversely with distance (approximately). For comparison, we plot in Figure 8c the observed H I surface density (Table 2) and the projected surface density of the dark isothermal *sphere* used by MCBF96 to model the circular velocity curve (their model D), rescaled by a large constant factor (47.7).

EDITOR: PLACE FIGURE 9 HERE.

The similarity between the H I and the dark matter surface density profiles seen in Figure 8c has been noticed before in other studies (e.g. Bosma 1978, 1981; Carignan & Beaulieu 1989; Broeils 1992) and has been interpreted as possible evidence that the H I and dark matter are somehow associated. Here, we see also a qualitative similarity between the observed H I surface density profile and the surface density profile of the additional disk matter required to make $Q(r) = 2$ (Fig. 8b). It is tempting to regard this as further evidence that the dark matter is distributed in a disk and follows relatively closely the distribution of neutral hydrogen. However, the increase in disk surface density required to make the swing amplifier work efficiently ($X = 3$ over most of the disk; Fig. 8a) would lower $Q$ even more, and would make the disk unstable to axisymmetric modes. Figure 9 shows the ratio of the surface density obtained by imposing $X(r) = 3$ to Kennicutt's (1989) critical surface density for star formation in disks. This ratio is well above unity for the entire disk, so we would expect to see evidence of active star formation in the outer H I disk if the swing amplifier was working. However, Meurer et al. (1999) did not detect any H$\alpha$ emission past $R_{\rm Ho}$. Their observations revealed only three faint H II regions near the Holmberg radius. These can be ionized by single late O or early A type stars and are much fainter than those typically used to trace star formation in galaxies (as done by, e.g., Kennicutt 1989). Therefore, at this point, it is unlikely that dark matter distributed in a disk can account for all the properties of NGC 2915 simultaneously.

Nevertheless, it would be interesting to see this type of argument, based on Toomre's (1964) $Q$ parameter and the presence of a spiral pattern, be used more often in spiral galaxies to test for the presence of substantial amount of unseen disk matter (see, e.g., Quillen & Pickering 1997; see also Quillen & Sarajedini 1998 for a similar application to intermediate-redshift galaxies).

### 6.2. Slowly Rotating Triaxial Dark Halos

Simulations of hierarchical structure formation in cold dark matter (CDM) universes predict that the dark halos around galaxies are triaxial in the mean, with some tendency to prolate shapes (Frenk et al. 1988; Warren et al. 1992; Dubinski & Carlberg 1991). The triaxiality and oblateness are slightly stronger in the outer parts, but are almost independent of the halo mass and of the ratio $V_r/\sigma_v$ (rotational velocity to velocity dispersion), indicating that the halos are supported by anisotropic velocity dispersions. The total angular momentum vector is nevertheless preferentially aligned with the minor axis of the mass distribution at all radii. When dissipation is included, the halos become more oblate while the flattening is unchanged (Dubinski 1994).

Observationally, the constraints on the shape of galactic halos remain weak. Polar-ring galaxies (e.g. Sackett et al. 1994) and the flaring (e.g. Olling 1995) and warping (e.g. Sparke 1984a) of the outer H I disk of spirals are usually used to constrain the three-dimensional structure of halos. Such studies often indicate flattened and sometimes triaxial dark halos (see also Becquaert & Combes 1997; Olling 1996) but are as yet inconclusive.

We now consider the possibility that the dark halo of NGC 2915 is triaxial, with its figure rotating slowly about the rotation axis of the H I disk, and that the H I bar and spiral arms are due to the forcing of the H I disk by this massive, extended, and rotating

triaxial halo. The halo would then act much like a very massive, slowly rotating bar. This would readily explain why there is a unique pattern speed for the bar and spiral arms and why the bar ends so far from corotation (see § 4). The situation which we are proposing is similar to that of rotating weak oval distortions in disks, which are able to maintain an open spiral pattern to large radii (see, e.g., Hunter et al. 1988). This is in contrast to a more conventional bar, where the quadrupole term decreases too rapidly outside corotation (where the bar ends) to maintain a spiral pattern. Hydrodynamical simulations of gaseous disks in large tumbling triaxial halos would be very useful to test our suggestion and to study the evolution of disks in such potentials.

The straight line of nodes of NGC 2915's warp (MCBF96) supports the suggestion of a triaxial halo. Displacements between the angular momentum vectors of the inner and outer regions of disks arise naturally in CDM models because of tidal torques. In an axisymmetric but flattened potential, the line of nodes would wrap quickly, but in a triaxial potential, the principal axes of the halo provide natural directions with which the warp can align (see Binney 1992 for a review of warps). Furthermore, an annulus of orbits circulating around the short axis of a triaxial halo becomes vertically unstable if the figure rotates, providing a natural way to excite a warp. However, this may happen too far out in the disk (outside corotation for prograde orbits) to be of interest here (Binney 1978, 1981; see also Sparke 1984b).

While the studies mentioned above (Frenk et al. 1988; Warren et al. 1992; Dubinski & Carlberg 1991; Dubinski 1994) have shown that dark halos in CDM cosmological simulations can be strongly triaxial and have well-defined angular momentum properties (with flat rotation curves extending down to the core), only the instantaneous shapes and rotational motions within the figures (streaming) have been studied. As far as we are aware, there has been no systematic study yet of the *figure* rotation of these triaxial halos.

EDITOR: PLACE FIGURE 10 HERE.

Pfitzner (1999, in preparation) recently began a study of the figure rotation of halos in a set of large dissipationless CDM structure formation simulations. The halos shape distribution varies systematically with both radius and mass, but for our current purposes it suffices to say that many halos are significantly triaxial, as in other studies. Following the orientation of each halo over time, Pfitzner finds that a subset of triaxial halos exhibit steady figure rotation about their minor axis. The statistics of how many halos in the simulations have figure rotation is confused by numerical resolution issues, but the fraction is clearly significant. To verify that these results are not due to transient phenomena, one of the rotating halo candidates was extracted from the simulations at a time near the final epoch ($\approx$13 Gyr), and it was evolved in isolation. The halo displayed no systematic change of density or shape over a time of 5 Gyr. Figure 10 shows that the figure of this triaxial halo rotates as a solid body with constant pattern speed over the entire time span. Hence, we conclude that at least some halos in these CDM simulations do exhibit genuine steady slow figure rotation over a Hubble time. However, because the halos formed are much more massive than that of NGC 2915, these simulations are not yet directly applicable to systems of that size. They do, however, suggest that an underlying triaxial dark halo with figure rotation could make an important contribution to the dynamics of the outer H I disk of some galaxies. If this is correct, it also offers another possibility to measure the shape of (triaxial) dark halos from detailed H I velocity field, using methods similar to those of Franx, van Gorkom, & de Zeeuw (1994).

The slow pattern speeds found in the present study and in the above simulations are interesting in the context of recent work by Miwa & Noguchi (1998). They made $N$-body simulations of barred galaxies in which the bars arose (1) spontaneously in marginally stable disks, and (2) through the effect of a tidal interaction in more stable disks. The

pattern speeds of the spontaneous bars are fast, with corotation near the ends of the bars, as generally expected in self-consistent systems. In the tidally induced bars, however, the pattern speeds are mostly much slower, and the bars appear to be limited by the ILR, rather than by corotation. In particular, any relatively large tidal disturbance leads to a slow pattern speed, independent of the original properties of the disk. These results may be relevant to the pattern speeds of the triaxial dark halos formed in CDM simulations, in which the triaxiality results at least partially from tidal effects during the aggregation of the halos.

Although more speculative, it may also be that triaxial halos are an essential ingredient in the formation of starbursts. We may then be witnessing in NGC 2915 the gradual buildup of a bulge, as gas driven to the center by the triaxial halo potential and the bar is slowly transformed into stars by the central starburst. However, the red diffuse stellar population detected by MMC94 argues for an even earlier burst of star formation. Nevertheless, if all the H I were turned into stars, NGC 2915 would appear very much like a normal spiral galaxy, with an "old" bulge and a young disk which obeys the Tully-Fisher relation (Tully & Fisher 1977; assuming $M/L_B = 1\ M_\odot/L_{B,\odot}$ for the gas). In this picture, the gaseous disk of NGC 2915 would be almost pristine.

## 7. Conclusion

We used the method of Tremaine & Weinberg (1984) to measure the disk pattern speed in the galaxy NGC 2915, using neutral hydrogen as the tracer and radio synthesis data. NGC 2915 is a BCD galaxy with a very extended H I disk showing an open barred spiral morphology. It is also strongly dominated by dark matter. Our measurements yield a pattern speed of $8.0 \pm 2.4$ km s$^{-1}$ kpc$^{-1}$ for $D = 5.3$ Mpc. This pattern speed is inconsistent with the general property of self-consistent barred disks that corotation occurs just outside

the end of the bar. However, it agrees well with more recent models considering dark halos with high central densities. Our adopted bar length puts corotation at more than 1.7 bar radii. We considered the possibility that the bar and spiral arms have different pattern speeds but demonstrated that this is unlikely.

Independent of the pattern speed measured, the existence of a bar and spiral pattern in NGC 2915 is also hard to explain. NGC 2915 is isolated, so gravitational interactions are unlikely to explain the strong pattern observed in the H I disk. Because the surface density in the disk is so low, Toomre's (1981) swing amplification mechanism is also unable to explain the origin of the structures. Furthermore, resonance ring theory fails to predict successfully the position of the pseudo-rings seen in the disk of NGC 2915, indicating that the spiral arms are not driven by the bar itself.

This lead us to consider two scenarios, involving different dark matter distributions, to explain both the structure and dynamics of NGC 2915's H I disk. Firstly, we considered dark matter in near-circular motion, distributed in a disk, and following closely the distribution of H I, as suggested by the similarity of the dark matter and H I surface density profiles. This does not appear to work: if the dark matter disk is dense enough for the swing amplifier to function efficiently, then the disk becomes unstable to axisymmetric disturbances and we would expect to see evidence of active star formation, which is not observed. Second, we considered the effects of dark matter distributed in a massive pressure-supported halo with extended triaxiality, like the halos seen in CDM cosmological simulations. In addition, we required the halo to have a slow figure rotation. Such figure rotation is seen in the preliminary analysis of a set of CDM simulations. These show triaxial halos with figure rotation constant over many Gyr. This kind of model has the potential to explain the structures seen in the disk of NGC 2915, through the torques exerted by the slowly rotating triaxial figure of the dark halo.

The structure in the H I disk of NGC 2915 is visible because the radio synthesis observations were made at a relatively high spatial resolution (beam FWHM of about 650 pc for the uniformly weighted data and about 1150 pc for the naturally weighted data). As far as we are aware, NGC 2915 is the only galaxy showing such structure in an extended H I disk. If our suggestions are correct, it would be very desirable to have H I observations of similar spatial resolution for other nearby galaxies with extended H I disks, as they may also provide similar insight into the dynamics of their dark halos. Our argument on figure rotation also relies heavily on the theory of forcing of structures by oval distortions, in a situation which is not precisely analogous to that in NGC 2915. Hydrodynamical simulations of gas disks in the potentials of triaxial halos with figure rotation would thus be very welcome.

We thank A. J. Kalnajs for comments on the manuscript and D. Pfenniger, J. A. Sellwood, and V. P. Debattista for useful discussions. M. Bureau acknowledges the support of an Australian DEETYA Overseas Postgraduate Research Scholarship and a Canadian NSERC Postgraduate Scholarship during the conduct of this research. The Digitized Sky Surveys were produced at the Space Telescope Science Institute under U.S. Government grant NAG W-2166. The images of these surveys are based on photographic data obtained using the Oschin Schmidt Telescope on Palomar Mountain and the UK Schmidt Telescope. The plates were processed into the present compressed digital form with the permission of these institutions.

## REFERENCES

Aoki, S., Noguchi, M, & Iye, M. 1979, PASJ, 31, 737

Athanassoula, E. 1992a, MNRAS, 259, 328

———. 1992b, MNRAS, 259, 345

Athanassoula, E., Bosma, A., & Papaioannou, S. 1987, A&A, 179, 23

Athanassoula, E., & Sellwood, J. A. 1986, MNRAS, 221, 213

Bardeen, J. M. 1975, in Dynamics of Stellar Systems, ed. A. Hayli (Reidel), 297

Becquaert, J.-F., & Combes, F. 1997, A&A, 325, 41

Begeman, K. G. 1989, A&A, 223, 47

Binney, J. J. 1978, MNRAS, 183, 779

———. 1981, MNRAS, 196, 455

———. 1992, ARA&A, 30, 51

Bosma, A. 1978, Ph.D. Thesis, University of Groningen

———. 1981, AJ, 86, 1971

Broeils, A. H. 1992, A&A, 256, 19

Byrd, G. G., Ousley, D., & Dalla Piazza C. 1998, MNRAS, 298, 78

Byrd, G., Rautiainen, P., Salo, H., Buta, R., & Crocker, D. A. 1994, AJ, 108, 476

Canzian, B. 1993, ApJ, 414, 487

Carignan, C., & Beaulieu, S. 1989, ApJ, 347, 760

Carignan, C., & Freeman, K. C. 1985, ApJ, 294, 494

Carr, B. 1994, ARA&A, 32, 531

Combes, F. 1993, in $N$-Body Problems and Gravitational Dynamics, ed. F. Combes & E. Athanassoula (Paris: Observatoire de Paris), 137

Combes, F., & Pfenniger, D. 1997, A&A, 327, 453

Combes, F., & Sanders, R. H. 1981, A&A, 96, 164

Contopoulos, G. 1980, A&A, 81, 198

Contopoulos, G., & Grosbøl, P. 1989, A&A Rev., 1, 261

Debattista, V. P., & Sellwood, J. A. 1998, ApJ, 493, L5

Dubinski, J. 1994, ApJ, 431, 617

Dubinski, J., & Carlberg, R. G. 1991, ApJ, 378, 496

Elmegreen, B. 1996, in Barred Galaxies, ed. R. Buta, D. A. Crocker, & B. G. Elmegreen (San Francisco:ASP), 197

Franx, M., van Gorkom, J. H., & de Zeeuw, T. 1994, ApJ, 436, 642

Frenk, C. S. White, S. D. M., Davis, M., & Efstathiou, G. 1988, ApJ, 327, 507

Gerin, M., Combes, F, & Athanassoula, E. 1990, A&A, 230, 37

Gerssen, J., Kuijken, K., & Merrifield, M. R. 1999, MNRAS, submitted.

Goldreich, P., & Lynden-Bell, D. 1965, MNRAS, 130, 125

Hunter, J. H., Ball, R., Huntley, J. M., England, M. N., & Gottesman, S. T. 1988, ApJ, 324, 721

Kalnajs, A. J. 1971, ApJ, 166, 275

———. 1977, ApJ, 212, 637

Kennicutt, R. C. Jr. 1989, ApJ, 344, 685

Kent, S. M. 1987, AJ, 93, 1062

———. 1990, AJ, 100, 377

Kormendy, J. 1984, ApJ, 286, 132

Kuijken, K., & Merrifield, M. R. 1996, in Barred Galaxies, ed. R. Buta, D. A. Crocker, & B. G. Elmegreen (San Francisco:ASP), 215

Lequeux, J., & Allen, R. J. 1993, A&A, 280, L23

Lindblad, P. A. B., & Kristen, H. 1996, A&A, 313, 733

Lindblad, P. A. B., Lindblad, P. O., & Athanassoula, E. 1996, A&A, 313, 65

Marlowe, A. T., Heckman, T. M., Wyse, R. F. G., & Schommer, R. 1995, ApJ, 438, 563

Merrifield, M. R., & Kuijken K. 1995, MNRAS, 274, 933

Meurer, G. R., Carignan, C., Beaulieu, S. F., & Freeman, K. C. 1996, AJ, 111, 1551 (MCBF96)

Meurer, G. R., Freeman, K. C., Bland-Hawthorn, J., Knezek, P. M., & Allen, R. J. 1999, BAAS, 31, 828

Meurer, G. R., Mackie, G., & Carignan, C. 1994, AJ, 107, 2021 (MMC94)

Miwa, T., & Noguchi, M. 1998, ApJ, 499, 149

Noguchi, M. 1987, MNRAS, 228, 635

Olling, R. P. 1995, AJ, 110, 591

———. 1996, AJ, 112, 481

Petrou, M., & Papayannopoulos, T. 1986, MNRAS, 219, 157

Pfenniger, D., & Combes, F. 1994, A&A, 285, 94

Pfenniger, D., Combes, F., & Martinet, L. 1994, A&A, 285, 79

Quillen, A. C., & Sarajedini, V. L. 1998, AJ, 115, 1412

Quillen, A. C., & Pickering, T. E. 1997, AJ, 113, 2075

Raha, N., Sellwood, J. A., James, R. A., & Kahn, F. D. 1991, Nature, 352, 411

Ryder, S. D., Buta, R. J., Toledo, H., Shukla, H., Staveley-Smith, L., & Walsh, W. 1996, ApJ, 460, 665

Sackett, P. D., Rix, H.-W., Jarvis, B. J., & Freeman, K. C. 1994, ApJ, 436, 629

Sancisi, R., Allen, R. J., & Sullivan, W. T. 1979, A&A, 78, 217

Schmidt, K.-H., & Boller, T. 1992, ANac, 313, 189

Schwarz, M. P. 1981, ApJ, 247, 77

———. 1984, MNRAS, 209, 93

Seiger, M. S., & James, P. A. 1998, MNRAS, 299, 672

Sellwood, J. A. 1980, A&A, 89, 296

——— 1981, A&A, 99, 362

Sellwood, J. A., & Sparke, L. S. 1988, MNRAS, 231, 25

Sellwood, J. A., & Wilkinson, A. 1993, Re. Prog. Phys., 56, 173

Sparke, L. S. 1984a, ApJ, 280, 117

———. 1984b, MNRAS, 211, 911

Sparke, L. S., & Sellwood, J. A. 1987, MNRAS, 225, 653

Sygnet, J. F., Tagger, M., Athanassoula, A., & Pellat, R. 1988, MNRAS, 232, 733

Tagger, M., Sygnet, J. F., Athanassoula, A., & Pellat, R. 1987, ApJ, 318, L43

Teuben, P. J., & Sanders, R. H. 1985, MNRAS, 212, 257

Toomre, A. 1964, ApJ, 139, 1217

———. 1981, in Structure and Evolution of Normal Galaxies, ed. S. M. Fall & D. Lynden-Bell (Cambridge: Cambridge University Press), 111

Tremaine, S., & Weinberg, M. D. 1984, ApJ, 282, L5

Trimble, V. 1987, ARA&A, 25, 425

Tully, R. B., & Fisher, J. R. 1977, A&A, 54, 661

Warren, M. S., Quinn, P. J., Salmon, J. K., & Zurek, W. H. 1992, ApJ, 399, 405

Weinberg, M. D. 1985, MNRAS, 213, 451

Wilson, T. L., & Mauersberger, R. 1994, A&A, 282, L41

This manuscript was prepared with the AAS LaTeX macros v4.0.

Fig. 1.— Meurer et al. (1996) naturally weighted total H I intensity map, overlaid on an optical image of NGC 2915 (Digitized Sky Survey). The beam is $45'' \times 45''$. Contours levels are 2.5, 7.5, 15, 25, 50, 75, and 90 percent of the peak H I surface brightness of 3.1 Jy beam$^{-1}$ km s$^{-1}$ ($N_{HI} = 1.71 \times 10^{21}$ cm$^{-2}$).

Fig. 2.— Meurer et al. (1996) naturally weighted H I velocity field, overlaid on an optical image of NGC 2915 (Digitized Sky Survey). The beam is $45'' \times 45''$, and the velocity resolution is 6.62 km s$^{-1}$. Contours are heliocentric velocities separated by 10 km s$^{-1}$. A few contours are identified on the map.

Fig. 3.— Schematised view of the "set-up" needed for the Tremaine-Weinberg method calculations (eq. [1]), overlaid on a grayscale image of Meurer et al. (1996) naturally weighted total H I intensity map ($45'' \times 45''$ beam).

Fig. 4.— Tremaine-Weinberg method measurements of the pattern speed in NGC 2915. (a) shows the case with Meurer et al. (1996) tilted-ring model best fit parameters, while (b) shows a typical good case. Parameters are indicated in the bottom left corner of each graph.

Fig. 5.— Calculated swing amplifier parameter $X(r)$ (eq. [5]) for two-armed ($m = 2$, full lines) and four-armed ($m = 4$, dotted lines) spiral patterns in NGC 2915. (a) shows $X(r)$ when only the H I distribution is taken into account, while in (b) both the H I and the stellar component are considered. $X \lesssim 3$ is required for swing amplification.

Fig. 6.— Calculated stability parameter $Q(r)$ (eq. [6]) in NGC 2915. The full line shows $Q(r)$ considering a fixed sound speed $v_s(r) = 8$ km s$^{-1}$, equal to the velocity dispersion in the outer parts of the H I disk, while the dotted line assumes $v_s(r) = \sigma_v(r)$. $Q(r)$ scales directly with $v_s(r)$. $Q \gtrsim 2$ curbs swing amplification.

Fig. 7.— (a) Calculated Lindblad precession frequencies for NGC 2915 (solid lines). From top to bottom, they are $\Omega + \kappa/2$, $\Omega$, $\Omega - \kappa/4$, and $\Omega - \kappa/2$ respectively. The dashed line shows the adopted pattern speed $\Omega_p$, while the dot-dashed lines show the range of values allowed by the uncertainty on $\Omega_p$. (b) is simply an enlargement of (a), but in addition the position of various features in the disk of NGC 2915 are indicated (dotted vertical lines).

Fig. 8.— (a) Calculated disk dark matter surface density needed to make the swing amplifier parameter $X(r) = 3$ (eq. [5]) for a two-armed ($m = 2$) spiral pattern in NGC 2915. The full line shows $\mu_{DM}$ when only the H I distribution is taken into account, while for the dotted line both the H I and the stellar component are considered. (b) Calculated disk dark matter surface density needed to make the stability parameter $Q(r) = 2$ (eq. [6]). The full line shows $\mu_{DM}$ considering a fixed sound speed $v_s(r) = 8$ km s$^{-1}$, while the dotted line assumes $v_s(r) = \sigma_v(r)$. $Q(r)$ scales directly with $v_s(r)$. (c) The full line shows $\mu_{\rm HI}$, the observed disk surface density of H I (Table 2), while the dotted line shows the projected dark matter surface density $\mu_{DM}$ of the dark isothermal sphere needed to model the rotation curve (model D of MCBF96, rescaled by 47.7).

Fig. 9.— Calculated ratio of the total surface density required to make the swing amplifier parameter $X(r) = 3$ (eq. [5] with $m = 2$) to the critical surface density required for star formation in galactic disks (Kennicutt 1989).

Fig. 10.— (a) Orientation of the major axis of a dark halo formed in a CDM simulation and evolved in isolation (see § 6.2) as a function of time. The angle $\theta$ is measured in a fixed plane perpendicular to the minor axis (the rotation axis). Filled circles show the mean orientation of the halo as a function of time, and the dotted line is a linear fit to the data. (b) Orientation of the major axis of the halo as a function of radius (in isodensity-defined shells) for selected times, showing that the halo rotates as a solid-body.

Table 1. Basic Properties of NGC 2915

| Quantity | Value | Reference |
|---|---|---|
| Position (J2000) | $\alpha = 9^{\rm h}26^{\rm m}11\overset{\rm s}{.}83$ | 1 |
| Position (J2000) | $\delta = -76°37'35\overset{''}{.}8$ | 1 |
| Heliocentric Velocity | $V_\odot = 468 \pm 5$ km s$^{-1}$ | 2,3 |
| Distance | $D = 5.3 \pm 1.6$ Mpc | 1 |
| Classification | I0/BCD | 1 |
| Total Apparent $B$ Magnitude | $m_{B_T} = 13.34$ mag | 1 |
| Total Absolute $B$ Magnitude | $M_{B_T} = -15.90$ mag | 1 |
| $B$ Disk Scalelength | $\alpha_B^{-1} = 25\overset{''}{.}6$ (660 pc) | 1 |
| Corrected $B$ Central Surface Brightness | $B(0)_c = 22.44$ mag arcsec$^{-2}$ | 1 |
| $B$ Holmberg Radius ($\mu_{B,0} = 26.6$ mag arcsec$^{-2}$) | $R_{{\rm Ho},B} = 1\overset{'}{.}9$ (2.93 kpc) | 1 |
| Total H I Flux | $F_{\rm HI} = 145$ Jy km s$^{-1}$ | 2 |
| Total H I Mass | $M_{\rm HI} = 9.58 \times 10^8\ M_\odot$ | 2 |
| H I Velocity Width | $W_{20} = 170$ km s$^{-1}$ | 2 |
| H I Extent ($N_{\rm HI,0} = 5 \times 10^{19}$ cm$^{-2}$) | $R_{\rm HI} = 9\overset{'}{.}7$ (14.9 kpc) | 2 |
| Dust Mass | $M_{\rm Dust} = 1.05 \times 10^4\ M_\odot$ | 3 |
| Total Mass (within $r \approx 600'' = 15.4$ kpc) | $M_{\rm Tot} = 2.7 \times 10^{10}\ M_\odot$ | 2 |

References. — (1) Meurer et al. 1994; (2) Meurer et al. 1996; (3) Schmidt & Boller 1992.

Table 2. Structural and Kinematical Profiles of NGC 2915

| $r$ (arcsec) | $\mu$HI ($M_\odot$ pc$^{-2}$) | $\mu_B$ ($B$ mag arcsec$^{-2}$) | $V_c$ (km s$^{-1}$) | $\sigma_v$ (km s$^{-1}$) | $\Omega$ (km s$^{-1}$ arcsec$^{-1}$) | $\kappa$ (km s$^{-1}$ arcsec$^{-1}$) |
|---|---|---|---|---|---|---|
| 27.5 | 8.90 | 22.55 | 39.0 | 33.4 | 1.42 | 2.37 |
| 52.5 | 6.35 | 23.97 | 53.0 | 28.8 | 1.01 | 1.76 |
| 77.5 | 4.10 | 25.11 | 65.0 | 23.0 | 0.84 | 1.44 |
| 102.5 | 3.17 | 26.26 | 72.7 | 20.8 | 0.71 | 1.15 |
| 127.5 | 2.53 | 27.20* | 76.0 | 15.6 | 0.60 | 0.93 |
| 152.5 | 2.26 | 28.26* | 79.2 | 11.9 | 0.52 | 0.81 |
| 177.5 | 2.32 | 29.32* | 81.4 | 10.7 | 0.46 | 0.69 |
| 202.5 | 2.36 | 30.38* | 82.5 | 9.9 | 0.41 | 0.60 |
| 227.5 | 2.12 | 31.44* | 82.8 | 9.2 | 0.36 | 0.48 |
| 252.5 | 1.75 | 32.50* | 80.4 | 10.1 | 0.32 | 0.41 |
| 277.5 | 1.49 | 33.56* | 80.4 | 10.1 | 0.29 | 0.42 |
| 302.5 | 1.41 | 34.62* | 80.9 | 9.3 | 0.27 | 0.38 |
| 327.5 | 1.46 | 35.68* | 80.7 | 8.7 | 0.25 | 0.35 |
| 352.5 | 1.43 | 36.74* | 80.8 | 8.3 | 0.23 | 0.34 |
| 377.5 | 1.23 | 37.80* | 82.0 | 8.8 | 0.22 | 0.32 |
| 412.5 | 1.09 | 39.28* | 82.3 | 8.6 | 0.20 | 0.30 |
| 457.5 | 0.89 | 41.19* | 83.8 | 8.1 | 0.18 | 0.28 |
| 502.5 | 0.67 | 43.10* | 85.5 | 8.1 | 0.17 | 0.28 |
| 547.5 | 0.48 | 45.01* | 88.5 | 8.1 | 0.16 | 0.29 |
| 592.5 | 0.32 | 46.92* | 93.9 | 7.7 | 0.16 | 0.30 |

*Extrapolated values from the exponential fit to the outer parts of the disk of MMC94.

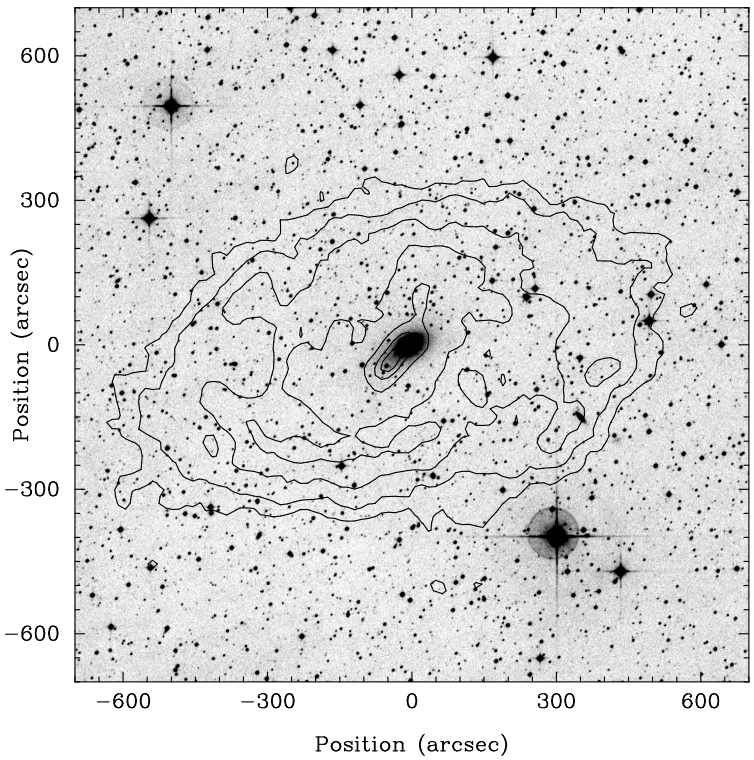
600
300
0
−300
−600
Position (arcsec)
−600
−300
0
300
600
Position (arcsec)

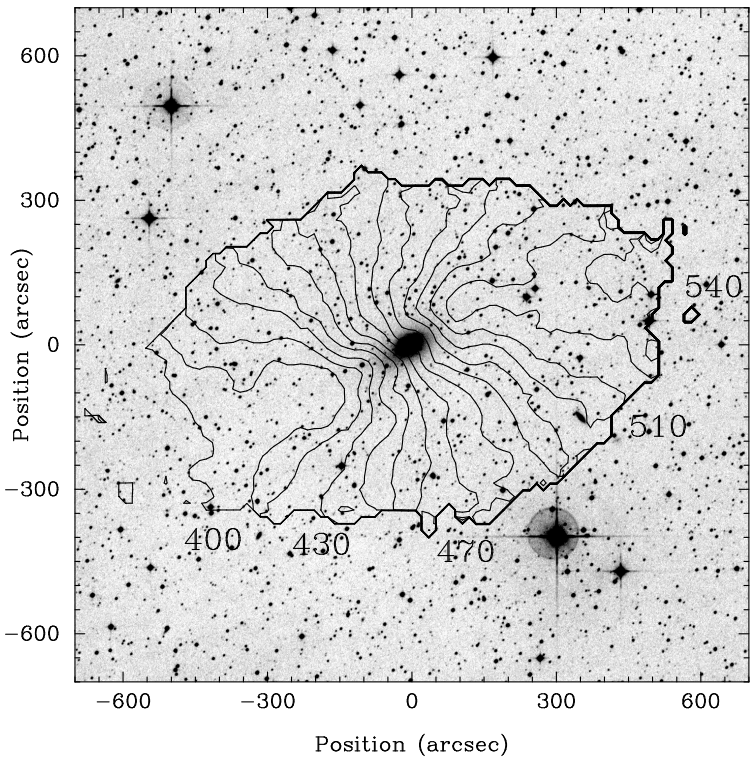
600
300
0
−300
−600
Position (arcsec)
−600
−300
0
300
600
Position (arcsec)
400
430
470
510
540

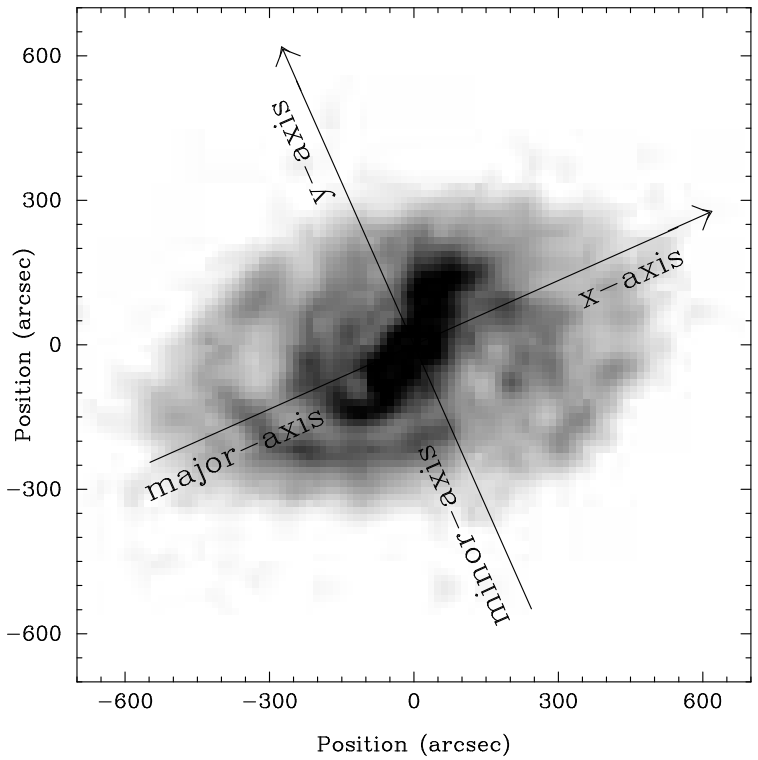
600
300
0
−300
−600
Position (arcsec)
−600
−300
0
300
600
Position (arcsec)
y−axis
x−axis
major−axis
minor−axis

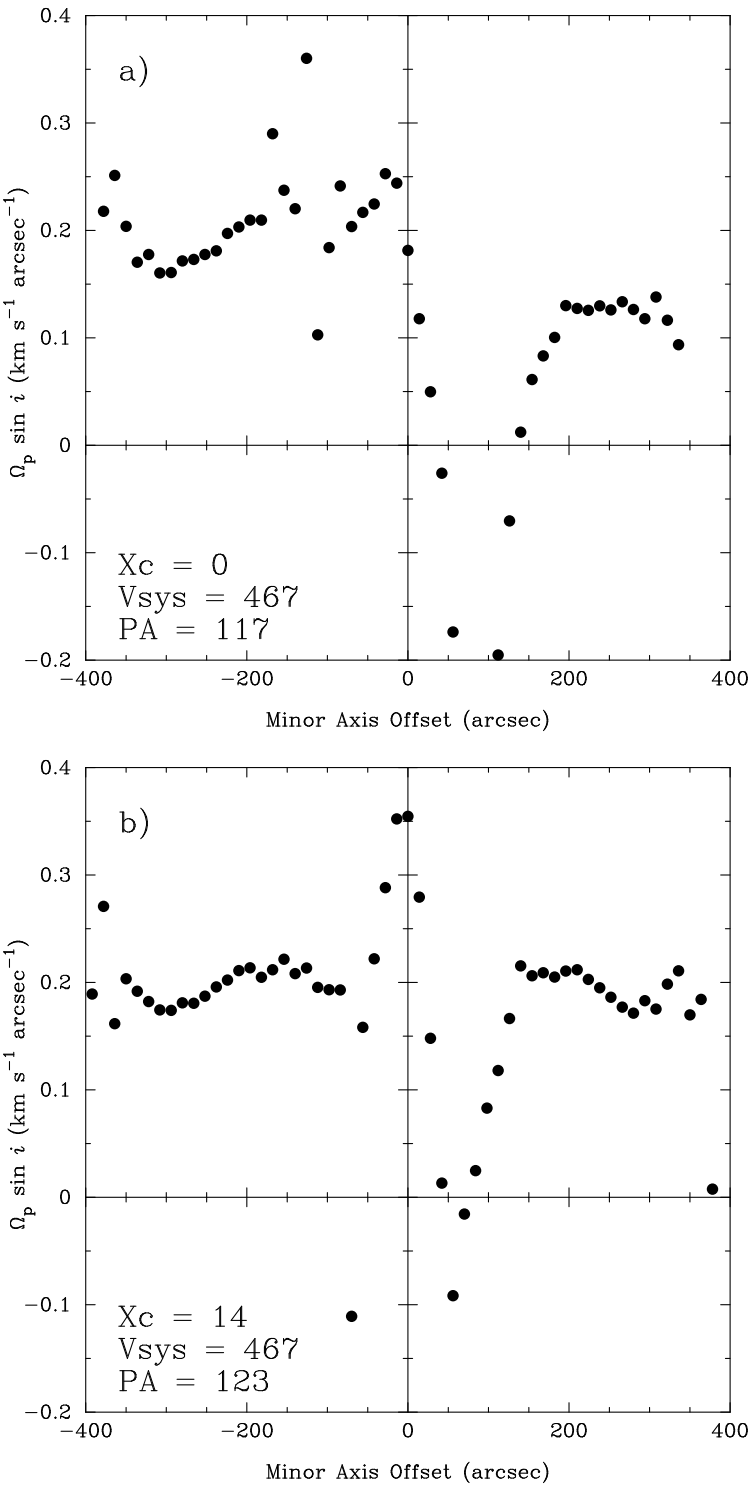
a)
Xc = 0
Vsys = 467
PA = 117
b)
Xc = 14
Vsys = 467
PA = 123
$\Omega_p$ sin $i$ (km s$^{-1}$ arcsec$^{-1}$)
Minor Axis Offset (arcsec)
0.4
0.3
0.2
0.1
0
−0.1
−0.2
−400
−200
0
200
400

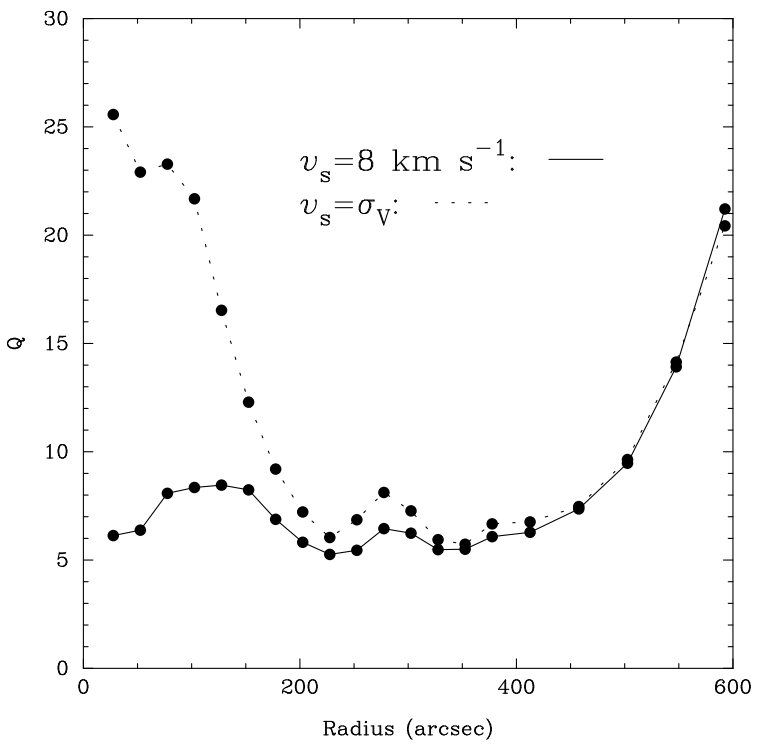
30
25
20
15
10
5
0
Q
0
200
400
600
Radius (arcsec)
$v_s$=8 km s$^{-1}$:
$v_s$=$\sigma_V$:

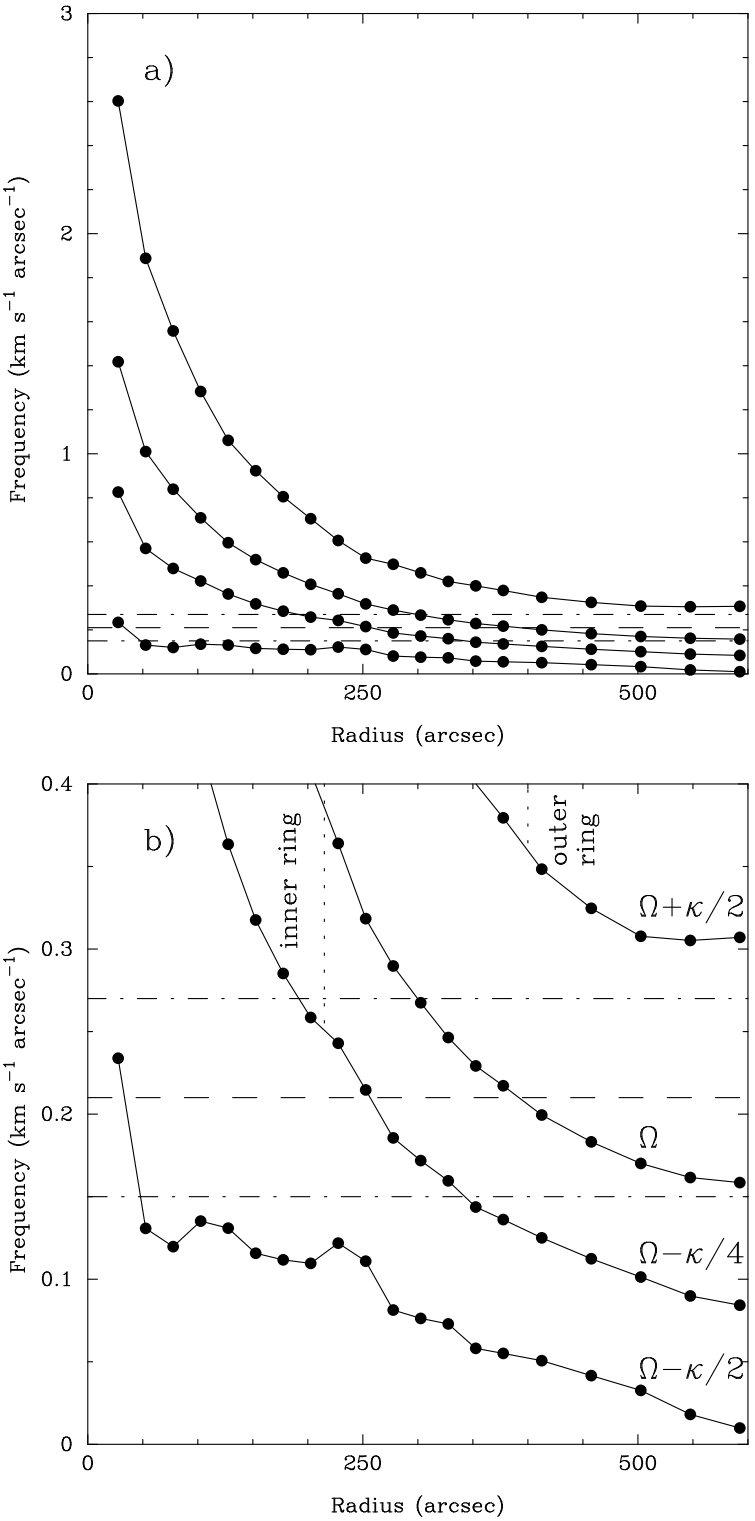
a)
Frequency (km s$^{-1}$ arcsec$^{-1}$)
Radius (arcsec)
0
250
500
1
2
3
b)
inner ring
outer ring
$\Omega+\kappa/2$
$\Omega$
$\Omega-\kappa/4$
$\Omega-\kappa/2$
0.1
0.2
0.3
0.4

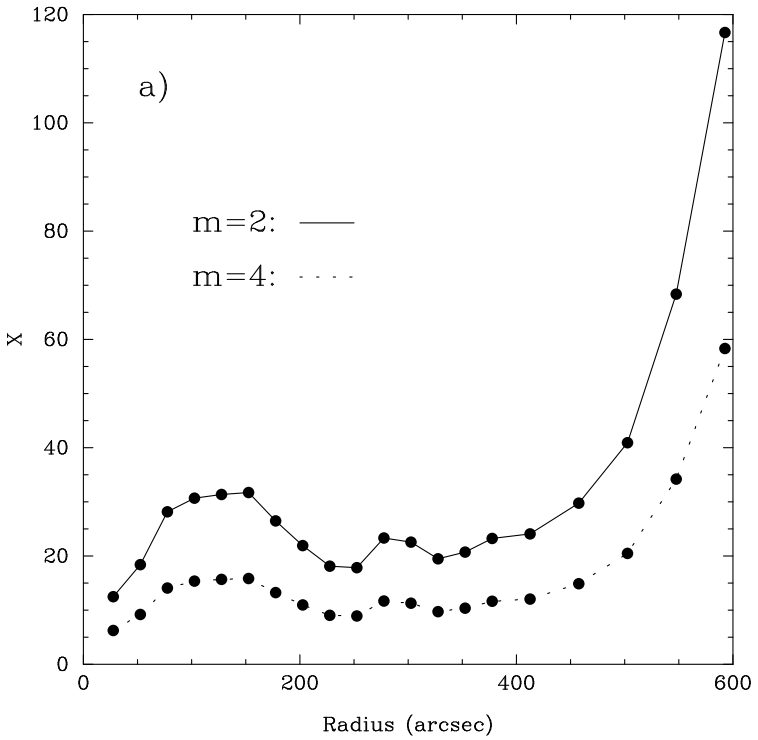
a)
m=2:
m=4:
X
Radius (arcsec)
0
20
40
60
80
100
120
0
200
400
600

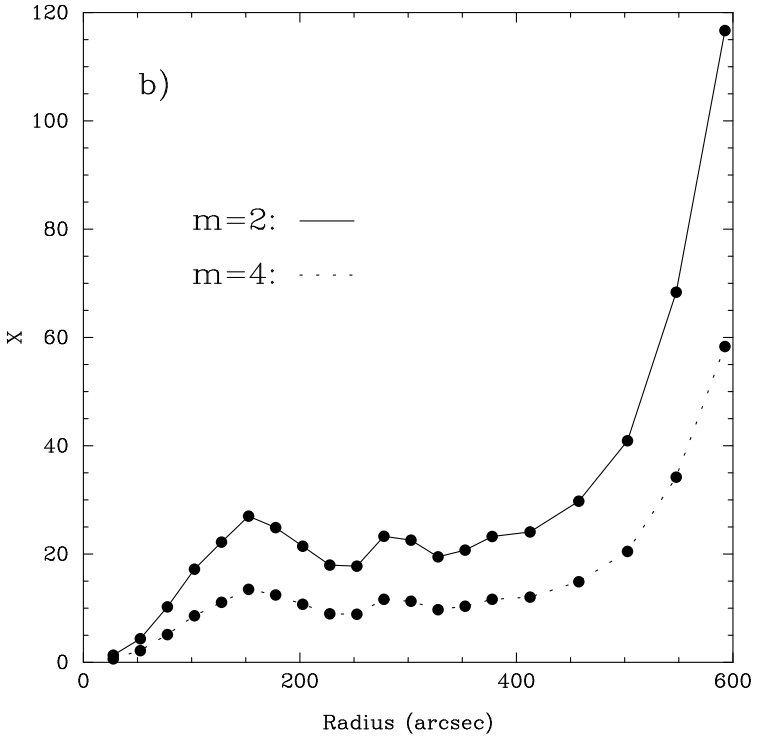
b)
m=2:
m=4:
X
Radius (arcsec)
0
20
40
60
80
100
120
0
200
400
600

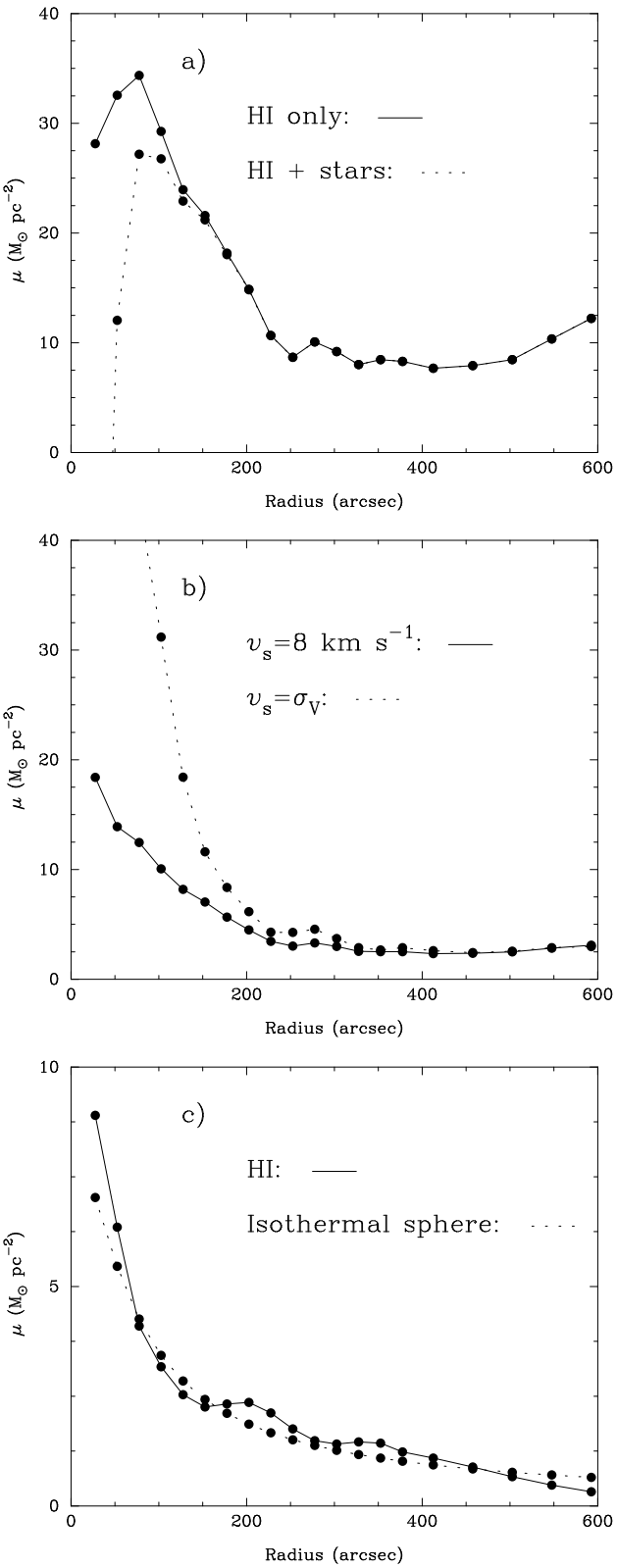
a)
HI only:
HI + stars:
μ (M⊙ pc⁻²)
Radius (arcsec)
b)
υs=8 km s⁻¹:
υs=σV:
μ (M⊙ pc⁻²)
Radius (arcsec)
c)
HI:
Isothermal sphere:
μ (M⊙ pc⁻²)
Radius (arcsec)

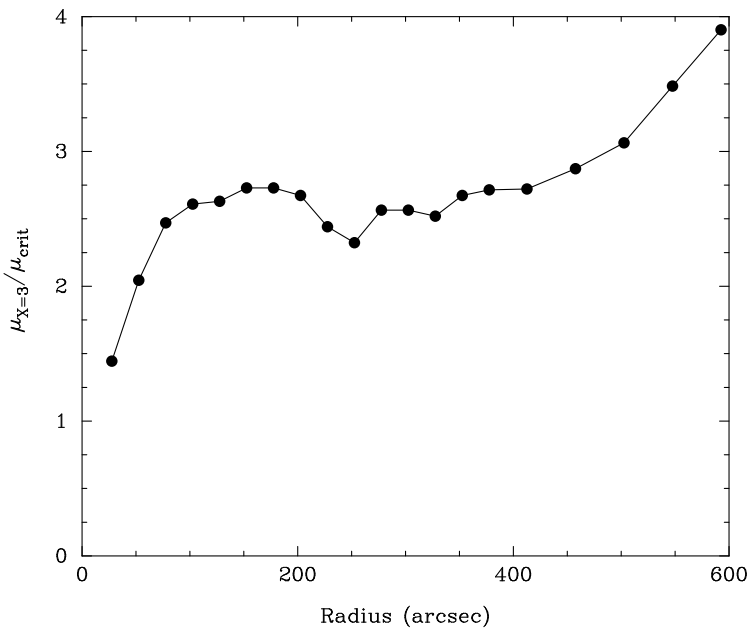
4
3
2
1
0
0
200
400
600
$\mu_{\chi=3}/\mu_{\rm crit}$
Radius (arcsec)

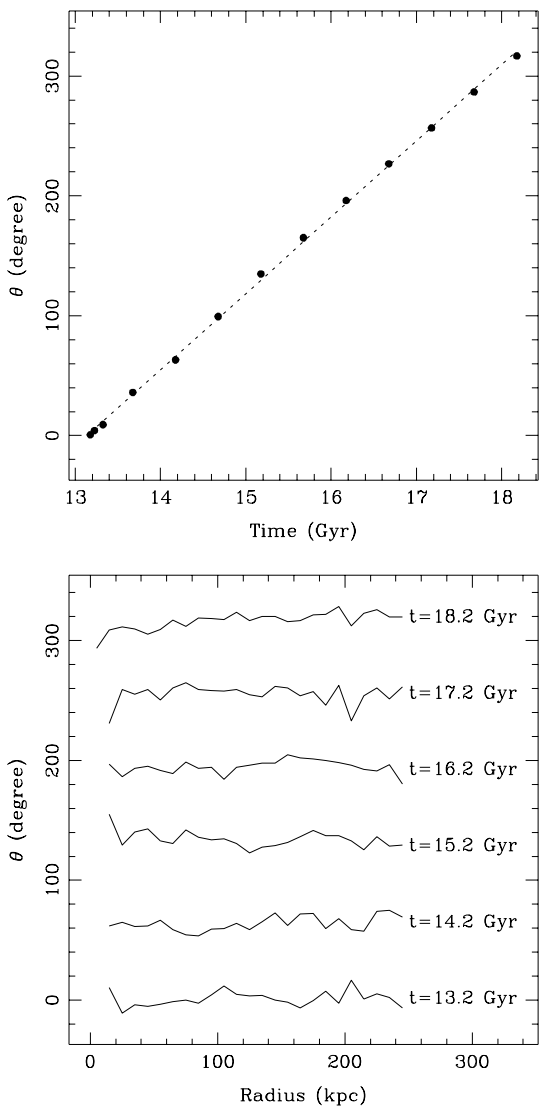
θ (degree)
Time (Gyr)
t=18.2 Gyr
t=17.2 Gyr
t=16.2 Gyr
t=15.2 Gyr
t=14.2 Gyr
t=13.2 Gyr
Radius (kpc)